Strong yet ductile steels via a heterogeneous phase transformation strategy

Ding, Ran; Yao, Yingjie; Sun, Binhan; Guo, Hui; Shao, Yang; Liu, Wei; Godfrey, Andy; Yang, Zhigang; Huang, Xiaoxu; Liu, Yongchang

DOI
10.1016/j.scriptamat.2024.116274

Publication date
2024

Document Version
Final published version

Published in
Scripta Materialia

Scripta Materialia 252 (2024) 116274

Contents lists available at ScienceDirect

Scripta Materialia

journal homepage: www.journals.elsevier.com/scripta-materialia

Strong yet ductile steels via a heterogeneous phase transformation strategy

Ran Ding [a,b], Yingjie Yao [a], Binhan Sun [c], Hui Guo [d], Jun Zhang [a], Yang Shao [a], Chi Zhang [a], Wei Liu [a], Andy Godfrey [a], Zhigang Yang [a], Xiaoxu Huang [e], Yongchang Liu [b], Sybrand van der Zwaag [a,f], Hao Chen [a,*]

[a] Key Laboratory for Advanced Materials of Ministry of Education, School of Materials Science and Engineering, Tsinghua University, Beijing 100084, PR China
[b] School of Materials Science and Engineering, Tianjin University, Tianjin 300354, PR China
[c] Max-Planck-Institut für Eisenforschung, Düsseldorf 40237, Germany
[d] School of Mechanical and Electrical Engineering, Guangdong University of Science and Technology, Dongguan 523083, PR China
[e] College of Materials Science and Engineering, Chongqing University, Chongqing 400044, PR China
[f] Faculty of Aerospace Engineering, Delft University of Technology, Delft, the Netherlands

ARTICLE INFO

Keywords:
Phase transformation
Metastable phase
Steel
Structural heterogeneity

ABSTRACT

A new route towards strong yet ductile metals via architecting heterogeneities in both structure and metastability is presented. Such heterogeneities are generated and manipulated in a standard stainless steel using a heterogeneous phase transformation (het-PT) strategy, in which focused laser patterning is applied to stimulate site-specific phase transformations. The het-PT processed steel contains periodically arranged stripes of strong martensite and ductile austenite with different grain sizes and metastability. The resulting structural heterogeneity leads to a desirable strain gradient and heterogeneous deformation-induced martensitic transformation during deformation, which effectively accommodate strain localization and enhance work hardening capability in the het-PT-processed steel. These unique features result in an enhanced balance between strength and ductility, outperforming both homogeneously ultrafine-grained and coarse-grained counterparts. The het-PT strategy is expected to be applicable to tailoring structural heterogeneity and metastability in other steels and metals.

Main text

Homogeneous ultrafine- and nano-grained metals can be exceptionally strong, as the high density of grain boundaries hinders dislocation transmission from one grain to another. The small grain size also, however, leads to a reduced dislocation mean free path and a decreased storage efficiency, resulting in a loss of ductility due to the deterioration in strain hardening ability [1-4]. Multiscale microstructural architecting by introducing a spatial heterogeneity in grain size, twinning spacing and phase constituents [5] has shown the potential to achieve an optimized combination of strength and ductility. Metallic materials with structural heterogeneities usually contain hard and soft regions with a large mechanical incompatibility. While hard regions provide high strength with a susceptibility to strain localization, soft ones promote strain gradients accommodated by geometrically necessary dislocations (GNDs) [6-10] or twins (GNTs) [11] to enhance overall strain hardening ability and suppress the propagation of shearing initiated nano-damage in hard regions [12-14]. Several approaches have been explored to generate structural heterogeneities. For instance, the application of surface mechanical attrition treatment, complemented by subsequent bulk annealing, can facilitate the introduction of a spatial gradient in grain size (or twinning spacing, and phase distribution) transitioning from the material's surface to its interior [5,7-9,12]. However, the extension of such gradient across additional geometric dimensions still remains challenging. The current methodologies do not offer the requisite flexibility to precisely control the spatial distribution of these heterogeneous components, thereby constraining the spectrum of achievable structural heterogeneities. Alternative approaches [15] should be explored to expand the dimensionality of structural heterogeneity architecting.

Metastability engineering, which provides a route to enhance strain hardening ability via deformation-induced martensitic transformation (DIMT), has proven to be another effective strategy to mitigate strength-ductility trade-off in various advanced alloys, such as high strength

* Corresponding author.
E-mail address: hao.chen@mail.tsinghua.edu.cn (H. Chen).

https://doi.org/10.1016/j.scriptamat.2024.116274
Received 10 April 2024; Received in revised form 11 July 2024; Accepted 14 July 2024
Available online 18 July 2024

steels, titanium alloys and high entropy alloys [16-19]. Strain hardening behavior can be effectively optimized via tuning mechanical stability of metastable phase, which governs DIMT during deformation. The most commonly used route to tailor metastable phase is through phase transformations during thermo-mechanical treatments. Such treatments, typically involving the use of a homogeneously applied heat treatment, result in a spatially random distribution of metastable grains with nearly uniform intrinsic stability, which necessarily implies that opportunities for additional strain hardening ability from use of an architectured metastability are unavailable.

Here we present an alternative strategy, namely heterogeneous phase transformation (het-PT) to enable multiscale (from nano- to meso-scale) microstructural architecturing. Via the manipulation of localized phase transformations in materials, this strategy allows us to efficiently design not only structural heterogeneity but also mechanical metastability. A fast laser patterning technique is used for localizing phase transformations via a controlled and spatially heterogeneous heat input. The laser scanned region, together with the surrounding heat affected zone is locally flash-heated, which leads to geometrically confined phase transformations, offering the het-PT-processed steel a substantially improved combination of tensile strength and ductility compared to that of homogeneous ultrafine-grained (UFG) or coarse-grained (CG) counterparts.

In order to demonstrate its potential, the het-PT strategy is benchmarked by application to a typical 304 stainless steel (SS304) sheet with an initially homogeneous martensitic microstructure (see experimental details of the starting material and the processing in Supplementary). SS304 has an excellent work hardening ability aided by the TRIP effect [20-22]. However, due to its low yield strength (~300 MPa) in the hot-wrought condition (Supplementary Fig. S1), further cold rolling and annealing are required to enhance the strength for use under severe load-bearing scenarios [23-25]. Heavily cold-rolled SS304 has a martensitic microstructure in a nano-lath (NL) like form (average interface spacing ~105 nm, Fig. 1a). After typical annealing, which allows a more ductile austenite to homogeneously form from the hard martensite, we can obtain an either coarse-grained (~3.2 μm) or ultrafine-grained (~330 nm) microstructure (H-CG or H-UFG samples, respectively, Fig. 1b and c) by adjusting the annealing time (i.e. 5 min and 2 h, respectively, see details in Supplementary). The ductility is thereby restored at the loss of some strength, which is determined by the grain sizes.

In contrast to the homogeneous microstructure obtained by annealing, the het-PT process can readily produce controlled heterogeneous structures at different length scales. The process is schematically represented in Fig. 1d. While a simple pattern of parallel lines with a constant spacing (up to the meso-scale millimeter range) along the rolling direction was applied to each surface of the cold-rolled SS304 sheet, an offset between the laser scan positions was used to achieve an alternating pattern of treatment in the cross section plane. The laser-induced localized temperature gradient results in the formation of a hierarchical microstructure (Fig. 1e–i). While the scanned region experiences fast melting and solidification (a depth of ~265 μm), yielding CG austenite

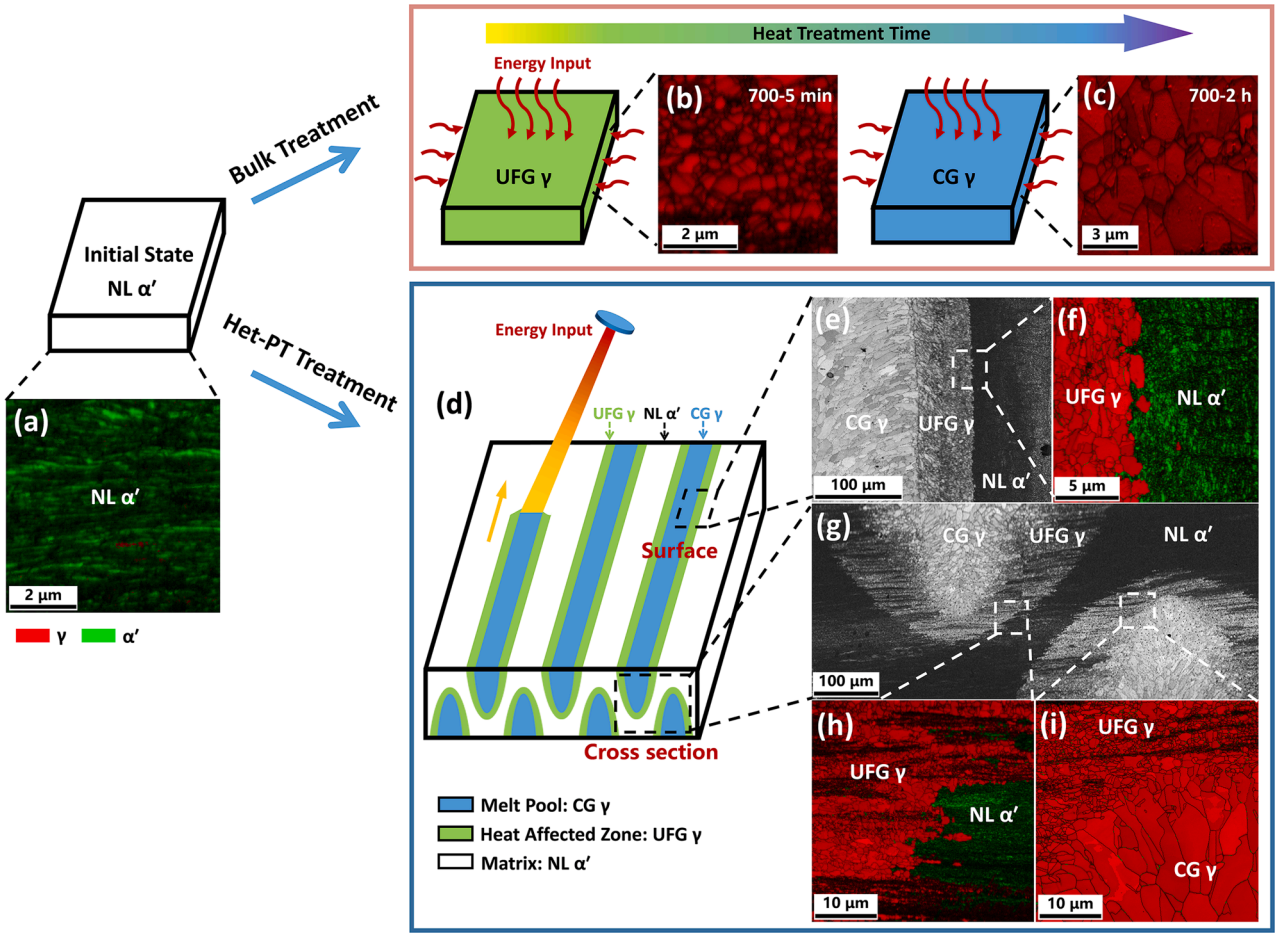

Fig. 1. Comparison of the het-PT strategy with conventional bulk annealing. (a) Cold rolled sheet with a nearly fully martensite microstructure. (b) Microstructure of the H-UFG sample, consisting of austenite grains of size ~330 nm. (c) Microstructure of the H-CG sample, consisting of austenite grains of size ~3.2 μm. (d) Schematic illustration of the het-PT process. (e) Representative microstructure of the three regions formed due to the het-PT process. (f) Enlargement of the area in (e). (g) Representative microstructure of the three regions formed due to the het-PT process as viewed in the cross-section. (h) and (i) are enlargements of the areas marked in (g).

in the form of columnar dendrites (Fig. 1e, average grain size ~11.7 μm), the heat affected zone around the melt pool undergoes rapid austenite reversion from martensite, leading to the formation of UFG austenite (Fig. 1f, average grain size ~670 nm). The NL martensitic microstructure remains unchanged in regions where the temperature increase is sufficiently small (Fig. 1f). As a result, regularly-spaced and periodically arranged bands of CG austenite, UFG austenite and NL martensite are developed at each scanned surface, and the alternating laser scan positions on the two surfaces lead to a phase arrangement on the transverse section resembling that of interlocked teeth (Fig. 1g).

Conventional annealing to control the microstructural fineness of SS304 invariably leads to a severe trade-off in strength versus ductility [24,26]. Tensile tests (Fig. 2a) show that the H-CG sample has a good ductility but a low yield strength of 468 MPa. Ultra-grain refinement throughout the material can substantially enhance the yield strength (YS) to 851 MPa, but with a corresponding loss of uniform elongation (UE) from 35.0 % down to 10.1 %. The early onset of localized deformation modes, as reflected by the distinct serrations in the tensile curve and extensive shear banding in the deformed microstructure (Supplementary Fig. S2), is an intrinsic drawback of UFG and nano-grained metallic materials, and arises due to a lack of strain hardening ability [27,28]. Furthermore, as compared with the H-CG sample, deformation-induced martensitic transformation (DIMT) is substantially suppressed in the H-UFG sample (transformed fraction of 52.1% vs. 3.1 %, Supplementary Fig. S2), as austenite is over-stabilized by grain refinement [29]. The limited extent of DIMT contributes to a weaker TRIP effect, further contributing to the low ductility of the H-UFG sample. Compared to the annealed samples, het-PT processed samples show a much better balance of strength and ductility. The sample with a line spacing of 0.5 mm (het-$PT_{0.5}$) has a UE comparable with that of the H-CG sample, while its YS is exceptionally enhanced to 679 MPa. Due to its pronounced strain hardening (Fig. 2b), its ultimate strength even surpasses that of the H-UFG sample (1034 MPa vs. 901 MPa). By increasing the line spacing to 0.75 mm (het-$PT_{0.75}$), the YS is further increased to 1073 MPa with a UE still higher than that of the H-UFG sample (26.2% vs. 10.1 %). It should also be noted that as compared with the homogeneous samples, i.e. H-UFG and H-CG, the enhancement of YS between two het-PT samples leads only to a marginal loss of UE, which means that the strength-ductility trade-off is substantially relieved by the het-PT strategy.

Unlike the microstructure of conventionally annealed samples, the alternating phase configuration in the het-PT samples resembles that of a uni-directional fiber-strengthened composite (Fig. 1d). From this analogy it can be assumed that the 'fibers' (CG and UFG austenite regions) and the 'matrix' (NL martensite matrix) experience an isostrain condition when loaded in the elastic region ($\varepsilon_{CG} = \varepsilon_{UFG} = \varepsilon_{NL}$, where ε denotes strain, and the subscript denotes the phase region). Thus, the overall YS is not solely dictated by the softest component (CG austenite regions), but should be evaluated using a rule of mixtures as the weighted total stress borne by the CG, the UFG austenite regions and the NL martensite matrix. This represents a theoretical upper bound of the YS, which cannot be achieved in a randomly mixed microstructure [30]. For the CG regions, cellular structures with an average diameter of ~570 nm are present inside the coarse austenite grains (Fig. 3b). Similar cellular structures have been widely observed in metallic materials fabricated by selective laser melting of metal powders [2,31]. The current study suggests that selective laser melting of a bulk material can also lead to formation of such a substructure, which is beneficial to strength as cellular boundaries can effectively hinder dislocation movement [32]. Additionally, we observed a high density of dislocations and twins in austenite grains in the CG regions (Fig. 3c and d), created by the very localized rapid solidification, making the hardness of the CG austenite regions in the het-PT sample (Fig. 3a) higher than that of the H-CG sample (~195 $HV_{0.05}$), even though the grains are much coarser (~11.7 μm vs. ~3.2 μm). The UFG austenite region in the het-PT sample also contains a large number of dislocations and twins, as well as extensive stacking faults (Fig. 3g). This is the result of the massive $\alpha' \rightarrow \gamma$ transformation induced by the fast heating in the heat affected zone. Under such conditions, the austenite grains inherit a high density of crystal imperfections (Fig. 3f) from the NL martensite [33]. The strong

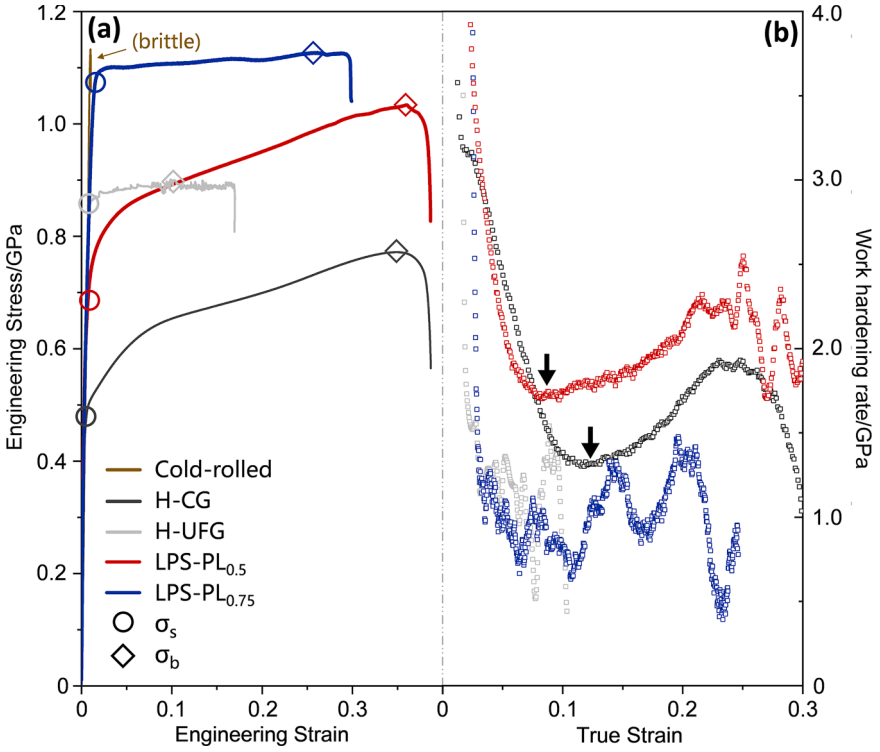

Fig. 2. Mechanical performance of samples fabricated by conventional annealing and het-PT strategy. (a) Engineering tensile curves and (b) work hardening rate curves. Arrows indicate the work hardening rate upturn of the H-CG and het-$PT_{0.5}$ samples.

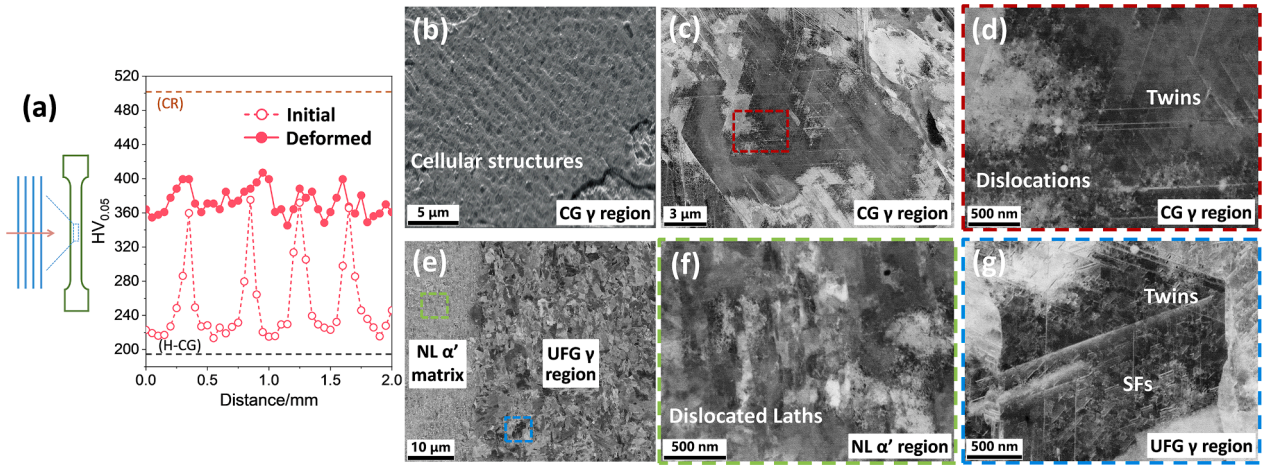

Fig. 3. Hardness and substructures of the het-PT processed sample. (a) Vickers hardness values across the scanned lines on the sheet surface of the het-$PT_{0.5}$ sample. (b) Cellular structures inside the CG region via SEM observation. (c) and (d) Microstructure of the CG region using electron channeling contrast imaging (ECCI), showing crystallographic imperfections inside the austenite grains. (e), (f) and (g) ECCI observations of the martensite matrix and UFG region. A considerable density of stacking faults (SFs), twins and dislocations are observed inside the austenite grain due to the fast reversion from deformed martensite. It should be noted that the NL martensite matrix shows a lower hardness than in the cold rolled condition due to the tempering caused by the temperature gradient induced by the laser processing.

CG and UFG austenite regions and the NL martensite matrix, are microscopically responsible for the high YS of the het-PT processed steel.

Fig. 4a and b show strain evolution in the gauge area of H-CG sample and het-$PT_{0.5}$ sample measured by digital image correlation (DIC). Appropriate speckle patterns were made upon the polished ND (normal direction) surface, where are imaged with a high resolution camera during the tensile test. The images were then analyzed using the VIC-2D software to generate strain distribution with respect to the reference image, i.e. the initial image taken of the specimen before any deformation. The details of the DIC setup are provided in Supplementary. It shows that a relatively homogeneous strain field is established throughout the observed gauge region of the H-CG sample, at the onset

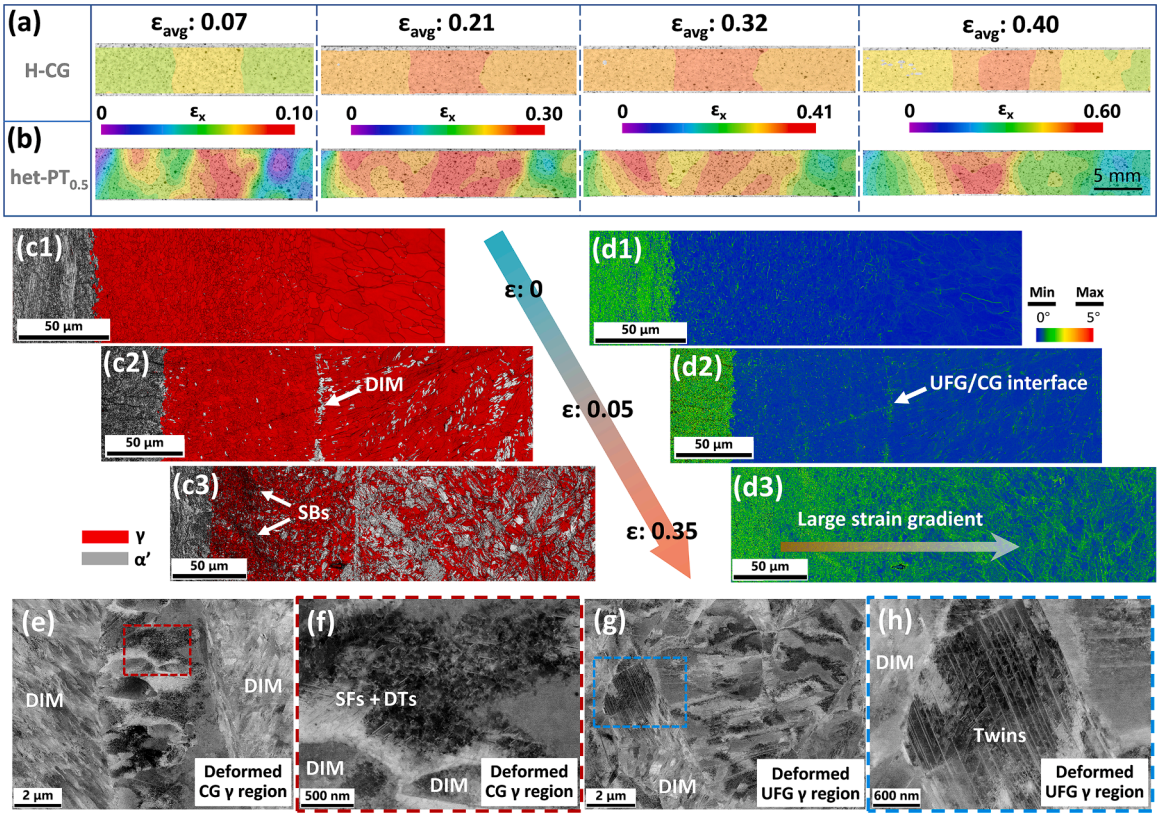

Fig. 4. Macro-scale, meso-scale and micro-scale mechanical response of the het-PT processed sample. Strain evolution in the gauge area of (a) H-CG sample and (b) het-PT0.5 samples measured by DIC. (c) EBSD maps revealing the evolution of the DIMT and the shear bands (SBs) during straining. Red regions represent austenite, while grey regions represent martensite. (d) KAM maps revealing the evolution of the strain gradient across different regions. (e), (f) and (g), (h) ECCI observations of the CG region and UFG region, respectively, after deformation, showing extensive deformation-induced lath martensite (DIM) and crystal imperfections, including stacking faults (SFs), twins and dislocations tangles (DTs). Note that ε-type martensite is rarely encountered.

of yielding, and each part of the strain field evolves uniformly during the tensile test before necking. In contrast, a varying pattern of multiple macroscopic strain localizations is observed as deformation proceeds in the het-$PT_{0.5}$ sample. The presence of strain concentration does not, however, lead to premature failure. Instead, the strain is transferred to other regions during continued loading. This heterogeneity in macroscopic strain-field evolution can be traced to the complex interaction between the diverse meso- and micro-mechanical responses of different regions (i.e. strain gradients, DIMT and micro shear bands) in the het-PT sample. When the het-PT samples start to yield, the NL martensite matrix and UFG austenite regions are expected to still be undergoing elastic deformation when the softer CG austenite regions begin to undergo plastic deformation. The plastically deforming CG austenite regions then have an apparent Poisson's ratio of 0.5, while that of other elastically deforming regions (martensite and UFG austenite) is still ~0.3 [34,35]. Consequently, the CG austenite regions tend to undergo a larger contraction than the NL martensite matrix and UFG austenite regions, which however is constrained by the well-bonded UFG austenite regions. This leads to preferential DIMT at the CG/UFG interfaces (Fig. 4c2), as the local stress state is altered from uniaxial to multiaxial. With further loading, the UFG austenite regions and the NL martensite matrix eventually yield. Due to the limited ductility (Fig. 2a), the NL martensite matrix would be expected to undergo fast necking at an early strain level. Again, however, the geometric constraint delays the onset of necking and also results in a multiaxial stress state at the UFG/NL interfaces [30], initiating shear bands towards the interior of the UFG austenite region (Fig. 4c3). Accordingly, the deformation incompatibilities among the different phase components generate a pronounced strain gradient inside the relatively soft region [6,7,36]. Kernel average misorientation maps (Fig. 4d), from electron backscatter diffraction (EBSD) data, provide evidence that a meso-scale strain gradient gradually builds up during deformation, from the NL martensite matrix towards the interior of the CG austenite region. Despite the presence of three phases with different strength, only a single extensive strain gradient is developed, as the high strength of the NL martensite matrix dominates the deformation response (Fig. 4d3).

The strain gradient in the het-PT processed sample leads to a distinctive DIMT behavior, especially in the UFG regions. As mentioned above, in the H-UFG sample shear banding prevails and nearly no DIMT occurs (Supplementary Fig. S3), resulting in a significant trade-off in ductility. Shear banding also takes place in the UFG region of the het-PT processed sample (Fig. 4c3). However, due to the geometric constraint of the heterogeneous structure architected by the het-PT process, propagation of shear bands is inhibited and catastrophic strain localization (i.e., necking) is effectively avoided. As a result, the extensive strain gradients and shearing in the UFG austenite region stimulate a considerable amount of DIM (~37.6 %, Fig. 4c3), even though the mechanical stability against such a transformation of UFG austenite containing a high density of crystal imperfections (Fig. 3g) is expected to be very high [37]. The local strain hardening ability is enhanced due to the TRIP effect, which in turn acts as a buffer to the strain accumulation, and stops shear bands from extending towards the CG regions (Fig. 4c3). The differences in the DIMT behavior of the UFG austenite in the het-PT processed and H-UFG samples indicates that the very stable UFG austenite grains can still transform to martensite if the local strain is sufficiently large [38-40], imposing a large mechanical driving force for the transformation. Under such circumstance, the pre-existing dislocations and twins in UFG austenite grains as the results of the laser processing (Fig. 3g) may serve as potential nucleation sites for martensitic transformation [41]. This is also supported by the observation of martensitic transformation in the severely deformed region near the fracture surface of the H-UFG sample (Supplementary Fig. S2). Such transformation, however, only occurs once necking is already well-developed in the H-UFG sample, where strain localization is irreversible. As a result of the developed strain gradient, the CG austenite regions in the het-PT processed samples also exhibit a higher fraction of DIM compared with the H-CG sample (63.9% vs. 52.1 %, Supplementary Fig. S3), despite the presence of a cellular structure [42,43]. The TRIP effect caused by DIMT leads to an upturn in the work hardening rate of the H-CG sample [44,45], while the combination of a large strain gradient and enhanced TRIP effect results in this upturn taking place earlier in the het-PT0.5 sample (Fig. 2b). It should be noted that the het-PT0.75 sample exhibits a relatively lower work hardening rate in comparison to the het-PT0.5 sample due to less austenitic regions. Yet, the competition between plastic instability and the TRIP effect offers the het-PT0.75 sample the ability to sustain a considerable Lüders-like strain before final fracture [41].

In general, the excellent work hardening capacity of the het-PT samples is to a large extent attributed to the promoted DIMT, though it is also worth noting that the heterogeneity in austenite metastability caused by the strain gradient and grain size difference may also play an important role. It is well accepted that to improve both strength and ductility in all TRIP-aided steels, a diverse austenite metastability is desired [46,47]. Otherwise, most DIMT would occur at a similar strain level, leading to rapid exhaustion of TRIP-aided work hardening ability, rather than allowing it to be exploited over a wide strain range. Our het-PT strategy can readily deploy austenite with a range of metastability. More importantly, the fractions of differently metastable austenite can be adjusted, which is not possible via the use of conventional thermomechanical treatments. Upon deformation, the DIMT occurs in the CG region first, followed by the DIMT in the UFG region, which offers het-PT processed samples the ability to bear the deformation heterogeneity (Fig. 4b).

To summarize, the het-PT strategy is highly versatile, and we envisage that it can be used to architecture desirable heterogeneous and potentially metastable microstructures as encountered in titanium alloys [46] and high entropy alloys [16,45] via localized phase transformations. Moreover, the fine spatial control available with laser patterning makes it possible to easily adjust the applied pattern to match the locally varying stress conditions [48] encountered in more complex application scenarios, and to obtain the highest resistance to crack initiation and propagation in the direction of the highest stresses. The great improvement in properties as demonstrated in this study on a simple and conventional SS304 serves as a stimulus to explore the landscape of the het-PT method for many more metallic systems showing solid state transformation in the sub minute scale.

CRediT authorship contribution statement

Ran Ding: Writing – review & editing, Writing – original draft, Visualization, Validation, Methodology, Investigation, Formal analysis, Data curation, Conceptualization. **Yingjie Yao:** Investigation, Formal analysis. **Binhan Sun:** Writing – review & editing, Methodology, Investigation, Formal analysis. **Hui Guo:** Investigation, Formal analysis. **Jun Zhang:** Investigation, Formal analysis. **Yang Shao:** Writing – review & editing, Methodology. **Chi Zhang:** Writing – review & editing, Writing – original draft, Methodology. **Wei Liu:** Writing – original draft, Resources. **Andy Godfrey:** Writing – review & editing, Writing – original draft, Resources, Methodology, Investigation. **Zhigang Yang:** Writing – review & editing, Writing – original draft, Resources, Methodology, Funding acquisition. **Xiaoxu Huang:** Writing – review & editing, Formal analysis. **Yongchang Liu:** Writing – review & editing, Resources. **Sybrand van der Zwaag:** Writing – review & editing, Writing – original draft, Methodology, Formal analysis, Conceptualization. **Hao Chen:** Writing – review & editing, Writing – original draft, Validation, Supervision, Software, Resources, Project administration, Methodology, Funding acquisition, Formal analysis, Conceptualization.

Declaration of competing interest

The authors declare that they have no known competing financial interests or personal relationships that could have appeared to influence

the work reported in this paper.

Acknowledgments

Financial support from National Key R&D program of China (Grant 2022YFE0110800 and 2022YFB3705300) is acknowledged. The authors are also grateful to the National Natural Science Foundation of China (grants 51922054, 52171008, 52171123 and 52104380) for grant and financial support.

Supplementary materials

Supplementary material associated with this article can be found, in the online version, at doi:10.1016/j.scriptamat.2024.116274.

References

[1] M.A. Meyers, A. Mishra, D.J. Benson, Mechanical properties of nanocrystalline materials, Prog. Mater. Sci. 51 (2006) 427–556.
[2] R. Song, D. Ponge, D. Raabe, J.G. Speer, D.K. Matlock, Overview of processing, microstructure and mechanical properties of ultrafine grained bcc steels, Mat. Sci. Eng. A-Struct. 441 (2006) 1–17.
[3] X.X. Huang, N. Hansen, N. Tsuji, Hardening by annealing and softening by deformation in nanostructured metals, Science 312 (2006) 249–251.
[4] M. Legros, B.R. Elliott, M.N. Rittner, J.R. Weertman, K.J. Hemker, Microsample tensile testing of nanocrystalline metals, Philos. Mag. A. 80 (2000) 1017–1026.
[5] X. Li, L. Lu, J. Li, X. Zhang, H. Gao, Mechanical properties and deformation mechanisms of gradient nanostructured metals and alloys, Nat. Rev. Mater. 5 (2020) 706–723.
[6] N. Fleck, G. Muller, M.F. Ashby, J.W. Hutchinson, Strain gradient plasticity: theory and experiment, Acta Metall. 42 (1994) 475–487.
[7] X. Wu, M. Yang, F. Yuan, G. Wu, Y. Wei, X. Huang, Y. Zhu, Heterogeneous lamella structure unites ultrafine-grain strength with coarse-grain ductility, Proc. Natl Acad. Sci. USA 112 (2015) 14501–14505.
[8] X.L. Wu, P. Jiang, L. Chen, T. Yun T. Zhu, Extraordinary strain hardening by gradient structure, Proc. Natl Acad. Sci. USA 111 (2014) 7197–7201.
[9] X.L. Wu, Y.T. Zhu, K. Lu, Ductility and strain hardening in gradient and lamellar structured materials, Scripta Mater. 186 (2020) 321–325.
[10] L.P. Kubin, A. Mortensen, Geometrically necessary dislocations and strain-gradient plasticity: a few critical issues, Scripta Mater. 48 (2003) 119–125.
[11] J.G. Sevillano, Geometrically necessary twins and their associated size effects, Scripta Mater. 59 (2008) 135–138.
[12] A. Misra, M. Goken, N.A. Mara, I.J. Beyerlein, Hierarchical and heterogeneous multiphase metallic nanomaterials and laminates, MRS Bull. 46 (2021) 236–243.
[13] X. Ma, C. Huang, J. Moering, M. Ruppert, H.W. Höppel, M. Göken, J. Narayan, Y. Zhu, Mechanical properties of copper/bronze laminates: role of interfaces, Acta Mater. 116 (2016) 43–52.
[14] I. Ibrahim, F. Mohamed, E. Lavernia, Particulate reinforced metal matrix composites—a review, J. Mater. Sci. 26 (1991) 1137–1156.
[15] S. Wei, C. Hutchinson, U. Ramamurty, Mesostructure engineering in additive manufacturing of alloys, Scripta Mater. 230 (2023) 115429.
[16] Z.M. Li, K.G. Pradeep, Y. Deng, D. Raabe, C.C. Tasan, Metastable high-entropy dual-phase alloys overcome the strength-ductility trade-off, Nature 534 (2016) 227–230.
[17] D. Raabe, Z.M. Li, D. Ponge, Metastability alloy design, MRS Bull 44 (2019) 266–272.
[18] Z.M. Li, C.C. Tasan, K.G. Pradeep, D. Raabe, A TRIP-assisted dual-phase high-entropy alloy: grain size and phase fraction effects on deformation behavior, Acta Mater. 147 (2017) 323–335.
[19] B. Ellyson, J. Klemm-Toole, K. Clarke, R. Field, M. Kaufman, A. Clarke, Tuning the strength and ductility balance of a TRIP titanium alloy, Scripta Mater. 194 (2021) 113641.
[20] P.L. Mangonon, G. Thomas, The martensite phases in 304 stainless steel, Metall. Trans. 1 (1970) 1577–1586.
[21] R. Lagneborgj, The martensite transformation in 18% Cr-8% Ni steels, Acta Metall. 12 (1964) 823–843.
[22] J. Venables, The martensite transformation in stainless steel, Philos. Mag. J. Theor. Exp. Appl. Phys. 7 (1962) 35–44.
[23] M. Naghizadeh, H. Mirzadeh, Microstructural evolutions during annealing of plastically deformed AISI 304 austenitic stainless steel: martensite reversion, grain refinement, recrystallization, and grain growth, Metall. Mater. Trans. A 47a (2016) 4210–4216.
[24] F. Forouzan, A. Najafizadeh, A. Kermanpur, A. Hedayati, R. Surkialiabad, Production of nano/submicron grained AISI 304L stainless steel through the martensite reversion process, Mat. Sci. Eng. A-Struct. 527 (2010) 7334–7339.
[25] A. Di Schino, J.M. Kenny, Grain size dependence of the fatigue behaviour of a ultrafine-grained AISI 304 stainless steel, Mater. Lett. 57 (2003) 3182–3185.
[26] G.S. Sun, L.X. Du, J. Hu, H. Xie, H.Y. Wu, R.D.K. Misra, Ultrahigh strength nano/ultrafine-grained 304 stainless steel through three-stage cold rolling and annealing treatment, Mater. Charact. 110 (2015) 228–235.
[27] Q. Wei, D. Jia, K.T. Ramesh, E. Ma, Evolution and microstructure of shear bands in nanostructured Fe, Appl. Phys. Lett. 81 (2002) 1240–1242.
[28] B.R. Kumar, D. Raabe, Tensile deformation characteristics of bulk ultrafine-grained austenitic stainless steel produced by thermal cycling, Scripta Mater. 66 (2012) 634–637.
[29] C.S. Yoo, Y.M. Park, Y.S. Jung, Y.K. Lee, Effect of grain size on transformation-induced plasticity in an ultrafine-grained metastable austenitic steel, Scripta Mater. 59 (2008) 71–74.
[30] H. Wu, G.H. Fan, An overview of tailoring strain delocalization for strength-ductility synergy, Prog. Mater. Sci. 113 (2020) 100675.
[31] Y.M. Wang, T. Voisin, J.T. McKeown, J.C. Ye, N.P. Calta, Z. Li, Z. Zeng, Y. Zhang, W. Chen, T.T. Roehling, R.T. Ott, M.K. Santala, P.J. Depond, M.J. Matthews, A. V. Hamza, T. Zhu, Additively manufactured hierarchical stainless steels with high strength and ductility, Nat. Mater. 17 (2018) 63–71.
[32] L. Liu, Q. Ding, Y. Zhong, J. Zou, J. Wu, Y.L. Chiu, J. Li, Z. Zhang, Q. Yu, Z. Shen, Dislocation network in additive manufactured steel breaks strength-ductility trade-off, Mater. Today 21 (2018) 354–361.
[33] H. Smith, D.R.F. West, The reversion of martensite to austenite in certain stainless steels, J. Mater. Sci. 8 (1973) 1413–1420.
[34] A. Wolfenden, K. Rahka, C. Laird, Poisson's ratio as determined for elastic and plastic deformation and for monotonic and cyclic loading—Part I: critical review, J. Test. Eval. 14 (1986) 173–180.
[35] M. Wiessner, E. Gamsjäger, S. van der Zwaag, P. Angerer, Effect of reverted austenite on tensile and impact strength in a martensitic stainless steel—An in-situ X-ray diffraction study, Mat. Sci. Eng. A-Struct. 682 (2017) 117–125.
[36] M. Ashby, The deformation of plastically non-homogeneous materials, Philos. Mag. J. Theor. Exp. Appl. Phys. 21 (1970) 399–424.
[37] B.B. He, M.X. Huang, On the mechanical stability of austenite matrix after martensite formation in a medium Mn steel, Metall. Mater. Trans. A 47a (2016) 3346–3353.
[38] W.W. Gerberich, P. Hemmings, V. Zackay, Fracture and fractography of metastable austenites, Metall. Mater. Trans. B 2 (1971) 2243–2253.
[39] S. Hazar, B. Alfredsson, J.B. Lai, Martensite transformation in the fatigue fracture surface of a high strength bearing steel, Eng. Fract. Mech. 220 (2019) 106650.
[40] A. Pineau, R. Pelloux, Influence of strain-induced martensitic transformations on fatigue crack growth rates in stainless steels, Metall. Trans. 5 (1974) 1103–1112.
[41] G.S. Sun, M.M. Zhao, L.X. Du, H.Y. Wu, Significant effects of grain size on mechanical response characteristics and deformation mechanisms of metastable austenitic stainless steel, Mater. Charact. 184 (2022) 111674.
[42] F.S.H.B. Freeman, J. Sharp, J.W. Xi, I. Todd, Influence of solidification cell structure on the martensitic transformation in additively manufactured steels, Addit. Manuf. 30 (2019) 100917.
[43] Y. Hong, C. Zhou, Y. Zheng, L. Zhang, J. Zheng, X. Chen, B. An, Formation of strain-induced martensite in selective laser melting austenitic stainless steel, Mat. Sci. Eng. A-Struct. 740 (2019) 420–426.
[44] M. Naghizadeh, H. Mirzadeh, Effects of grain size on mechanical properties and work-hardening behavior of AISI 304 austenitic stainless steel, Steel Res. Int. 90 (2019) 1900153.
[45] A.K. De, J.G. Speer, D.K. Matlock, M.C. Mataya, R.J. Comstock, Deformation-induced phase transformation and strain hardening in type 304 austenitic stainless steel, Metall. Mater. Trans. A 37a (2006) 1875–1886.
[46] M.M. Wang, C.C. Tasan, D. Ponge, D. Raabe, Spectral TRIP enables ductile 1.1 GPa martensite, Acta Mater. 111 (2016) 262–272.
[47] R. Ding, Z. Dai, M. Huang, Z. Yang, C. Zhang, H. Chen, Effect of pre-existed austenite on austenite reversion and mechanical behavior of an Fe-0.2 C-8Mn-2Al medium Mn steel, Acta Mater. 147 (2018) 59–69.
[48] H.S. Oh, J. Kang, C.C. Tasan, Enhancing damage-resistance in low carbon martensitic steels upon dual-pass laser treatment, Scripta Mater. 192 (2021) 13–18.